Digital Signal Processing 126 (2022) 103491

Contents lists available at ScienceDirect

Digital Signal Processing

www.elsevier.com/locate/dsp

Improved parametrized multiple window spectrogram with application in ship navigation systems

Denis Selimović [a], Jonatan Lerga [a,b,*], Péter Kovács [c,**], Jasna Prpić-Oršić [a]

[a] Department of Computer Engineering, Faculty of Engineering, University of Rijeka, Vukovarska 58, 51000 Rijeka, Croatia
[b] Center for Artificial Intelligence and Cybersecurity, University of Rijeka, Radmile Matejcic 2, 51000 Rijeka, Croatia
[c] Department of Numerical Analysis, Eötvös Loránd University, Pázmány Péter stny. 1/C, 1117 Budapest, Hungary

ARTICLE INFO

Article history:
Available online 25 February 2022

Keywords:
Time-frequency analysis
Multiple windows
Hermite functions
Variable projection
Rényi entropy
Ship navigation

ABSTRACT

In analyzing non-stationary noisy signals with time-varying frequency content, it's convenient to use distribution methods in joint, time and frequency, domains. Besides different adaptive data-driven time-frequency (TF) representations, the approach with multiple orthogonal and optimally concentrated Hermite window functions is an effective solution to achieve a good trade-off between low variance and minimized stable bias estimates. In this paper, we propose a novel spectrogram method with multiple optimally parameterized Hermite window functions, with parameterization which includes a pair of free parameters to regulate the shape of the window functions. The computation is performed in the optimization process to minimize the variable projection (VP) functional problem. The proposed parametrized distribution method improves TF concentration and instantaneous frequency (IF) estimation accuracy, as shown in experimental results for synthetic signals and real-life ship motion response signals. With the optimization of nonlinear least-squares approximation of the ship response signals, the Hermite spectra are centralized, and only up to 15 basis functions are sufficient for concentration improvement in the TF domain.

1. Introduction

To analyze changes in spectral densities over time, time-frequency distribution (TFD) methods are utilized, thus decomposing a signal in both the time and frequency domains. There are many different TFD methods for analyzing non-stationary noisy signals with time-varying frequency content. The analysis is performed using the spectrogram, or, more recently, any member of Cohen's class of TFDs. The spectrogram is characterized by simplicity; however, it does not provide satisfactory time-frequency (TF) resolution. On the other hand, Cohen's class quadratic TF distributions, as Wigner distribution, give satisfactory TF resolution but introduce undesired TF cross-term components [12]. Over the years, various advanced affined and reassigned TF methods have been developed to achieve finer properties such as localization, positivity, removal of unwanted cross-terms, etc. Usually, the choice of an appropriate method is data-driven and requires additional processing to obtain a trade-off between time and frequency resolution and to eliminate undesirable cross-terms [28].

Although adaptive TFD methods improve TF representations, bias and variance control issues are generally not considered. To maintain the favorable localization properties of conventional TF methods and improve the TF concentration, one can find different approaches in the literature. One solution to minimize the variance is to combine empirical methods with additional post-processing algorithms, e.g., the S-method with adaptive window-width selection [31]. On the other hand, an analysis approach with multiple orthogonal and optimally concentrated window functions has proven to be suitable for achieving minimal variance and bias while retaining favorable properties for non-stationary signals [8]. In other words, obtaining a good trade-off between low variance and minimized stable bias estimates can be done by applying the multiple windows (MW) approach. With favorable properties, the MW approaches to signal spectrum estimation found application in various fields such as radar imaging applications [23], vibration characterization in swallowing acceleration signals [22], classification [25], biomedicine [19] and many others.

To improve the concentration, one needs to choose the type and the number of applied window functions in the MW approach. In

* Corresponding author at: Faculty of Engineering and Center for Artificial Intelligence and Cybersecurity, University of Rijeka, Radmile Matejcic 2, 51000 Rijeka, Croatia.
** Corresponding author at: Department of Numerical Analysis, Eötvös Loránd University, Pázmány Péter stny. 1/C, 1117 Budapest, Hungary.
E-mail addresses: dselimovic@riteh.hr (D. Selimović), jlerga@riteh.hr (J. Lerga), kovika@inf.elte.hu (P. Kovács), jasnapo@riteh.hr (J. Prpić-Oršić).

https://doi.org/10.1016/j.dsp.2022.103491

addition to an appropriate choice of the number of window functions, the performance can be further improved by optimizing the weight coefficients of the MW distributions. In their work, [27] proposed a method to reduce the normalized mean squared error (MSE) by individually optimizing the weight coefficients. The method shows improvement in the final mean representation with scaling optimization. Also, [24] proposed optimized weight coefficients to improve instantaneous frequency (IF) estimates in a noisy environment. In the proposed approach, improvements in IF estimation accuracy were proved by calculating mean MSE values. The method demonstrated improvement for different signal to noise ratio (SNR) values and is suitable for use in a noisy environment.

In addition to modified (adopted) weight coefficients, the shape of the window functions could also be of great importance for optimizing MW distribution approaches. For example, [17] proposed a peak-matched MW approach to obtain low bias estimates in the vicinity of the peak frequency, with Karhunen-Loève basis functions of a known peaked spectrum used in the matching process. However, due to the finite length of the windows, leakages occur at frequencies outside the resolution bandwidth, so it is necessary to use the penalty function to suppress them. On the other hand, Hermite functions, as orthogonal and optimally concentrated window functions, have been shown to be very well suited to model compactly supported waveforms, such as blood pressure signals [19], QRS-complexes [26], or evoked potentials [6]. More recently, these models have been extended to include free parameters that allow the system of Hermite functions to be adapted to other signal processing problems, such as ECG delineation [5], data compression [19], and model-driven representation learning [18].

Optimizing free parameters affects the shape of the Hermite window functions. Therefore, it can be assumed that adapted window functions in the MW approach can potentially improve TF concentration and IF estimation accuracy. In this paper, we propose a novel parametrized multiple window spectrogram (MWS) method. The parameterization is given with pair of free parameters to minimize the variable projection (VP) functional problem, and the computation is performed in the optimization process. We observe mono- and multi-component signals with slowly varying frequency content. A noisy environment is modelled by adding white Gaussian noise, and signals are analyzed for different SNR values. We regulate the shape of the window functions by using only two free parameters. This affects the final optimization and results in TF representation improvement. In the evaluation process, the mean MSE of IF estimation is calculated for different types of synthetic signals with slowly varying frequencies, showing the improved accuracy of the IF estimation in noisy scenarios compared to original competitive methods. In addition, TF concentration is measured using the Rényi entropy, and it was shown that the proposed technique outperforms standard distributions both for synthetic and real-world ship motion response signals.

The rest of the paper is structured as follows. Section 2 provides a theoretical background of TFD approaches for non-stationary signals as well as MW analysis approaches in the TF domain with appropriate Hermite window functions. Section 3 explains the novel parameterization method with two free parameters, with their optimization to achieve improved representation results. Section 4 provides an insight into the efficiency of the proposed parametrized method, which is demonstrated in several synthetic and real-life experimental results. Discussion and concluding remarks are given in Section 5.

2. Theoretical background

Different versions of TFD methods have been proposed and used for processing of non-stationary signals, and, depending on the application, these methods are adopted to achieve the highest possible resolution and concentration in the time and frequency domains simultaneously, according to the uncertainty principle [9]. The resulting adaptive data-driven TF analysis methods are obtained using various non-parameterized and parameterized approaches [28]. The TF representation, well-known as a spectrogram, is traditionally used in practice due to its simplicity in realization and application. It represents the square modulus of the short-time Fourier transform (STFT) given by the following equation:

$$STFT(t,f) = \int_{-\infty}^{\infty} s(\tau)h(\tau - t)\mathrm{e}^{-j2\pi f\tau}d\tau, \tag{1}$$

where $s(\tau)$ is a considered signal, $h(t)$ is a fixed-size window function ($h(\tau - t)$ is the window function centered at t with τ denoting free variable). The optimal window length depends on the application and directly affects the time and frequency resolution. With larger values of window length, we divide the frequency range into smaller pieces. So any given sample is covered by more frames. It provides an improvement in frequency resolution (narrowband spectrogram). However, we have less precision in the time domain (blurring over time) because large values of window length integrate over longer windows of time. On the other hand, with a shorter window length, each frame only catches a small amount of information, and the precision of the transition location is much better, but the frequency resolution is intruded since the range is divided into only a few pieces (wideband spectrogram). In short, the time resolution is proportional to the effective duration, and the frequency resolution is proportional to the effective bandwidth of the observed analysis window. Moreover, it is possible to use additional arguments when calculating the STFT, such as the number of overlapping samples or the corresponding hop length. With a good choice of hop length, we can ensure that no information is lost in the STFT calculation and that the resulting STFT varies smoothly. The recommendation for selecting hop length values is to set the length as a fraction of window length, typically $\frac{1}{8}$, $\frac{1}{4}$, or $\frac{1}{2}$. For example, when using the Hanning window, an overlap length of 50 % is a good choice to reduce the variance of the spectral density calculated by the spectrogram. However, the spectrogram suffers from insufficiently high TF resolution, and it is not always suitable for advanced real-world signal analysis.

To improve the TF resolution, one can next use the quadratic (energy) TFDs. As the fundamental TFD method for all other energy distributions, Wigner-Ville distribution (WVD) is given as:

$$WVD(t,f) = \int_{-\infty}^{\infty} s(t+\frac{\tau}{2})s^*(t-\frac{\tau}{2})\mathrm{e}^{-j2\pi f\tau}d\tau. \tag{2}$$

It can provide a good time-frequency representation for chirp signals but produces cross-terms (the undesirable TF components), especially in the case of multi-component signals. On the other hand, the highly efficient S-method (obtained by simple convolution within the frequency-domain windows) reduces the cross-term phenomenon while preserving the concentration of the auto-terms in the TF plane. The S-method is given as follows [30]:

$$SM(t,f) = 2\int_{-\infty}^{\infty} P(\theta)STFT(t,f+\theta)STFT^*(t,f-\theta)d\theta. \tag{3}$$

By sliding the window width $P(\theta)$, one can perform a transition from a spectrogram to a WVD (so-called the smoothing process). With a narrow window, we get the blurred image, whereas a too

wide window can introduce cross-terms. Therefore, choosing the appropriate window width is necessary to simultaneously achieve acceptable TF resolution and reduce unwanted cross-terms.

To achieve a variety of properties as localization, positivity, cross-term removal, and other goals in TF analysis, other adaptive Cohen class quadratic distributions with smoothing kernels were designed [12]. However, in the development of adaptive TF methods with smoothing kernels, issues of bias and variance control are generally not considered [3]. For example, empirical WVD is unbiased, but it has infinite variance. To achieve minimal variance and bias while retaining favorable properties for non-stationary signals, one can use the TFD approach with MW functions. The MW approaches to signal spectrum estimation found applications in various fields, and many of these methods are based on Thomson's MW spectrum estimation technique for stationary signals [33]. Thomson's method proved very favorable localization properties using optimal window functions as discrete prolate spheroidal sequences (DPSS) [29]. However, the proposed method is restricted to stationary signals only and has a limited range of applications. In other words, DPSS window functions do not have optimal properties when non-stationary signals are observed in the joint time and frequency domain. MW approaches in analyzing non-stationary signals perform averaging over MW functions using orthogonal Hermite window functions. Hermite functions have become popular due to the very favorable properties of orthogonality (to achieve minimization of variance), optimal TF concentration (to perform stable bias estimations), and simple implementation. Various MW approaches in TF analysis of non-stationary signals have been developed to improve the representation of spectral components with both minimal variance and stable bias estimates. The MWS approach has also emerged as an improvement to Thomson's method. For signal $s(t)$, it is defined as the weighted sum of K spectrograms as follows:

$$MWS_K(t,f) = \sum_{k=0}^{K-1} d_k(t) S_k(t,f), \tag{4}$$

where $d_k(t)$ are weight coefficients, and $S_k(t,f)$ is the spectrogram obtained according to the given Hermite window function $h_k(t)$ of k-th order [8]:

$$S_k(t,f) = \left| \int_{-\infty}^{\infty} s(\tau) h_k(\tau - t) e^{-j2\pi f\tau}\, d\tau \right|^2. \tag{5}$$

The estimate of the time-varying spectrum is defined here as the weighted sum of the individual estimates in each quasi-stationary segment, indexed by time. In other words, fitting locally stationary processes in particular segments of limited duration are achieved, and then averaging by weighted sum is performed. More window functions provide a higher concentration in the TF plane, resulting in lower variance. However, we also want to maintain a high resolution. For this purpose, using an optimal number of Hermite window functions and adjusted weighting coefficients is of great importance. Therefore, the change in the number of windows K should be followed by an appropriate adjustment to achieve a trade-off between bias and variance. In other words, optimizing and controlling the given trade-off is done by regulating the number of the orthogonal windows and adjusting the weighting coefficients.

As mentioned before, DPSS window functions are not suitable for observing signals in the joint TF domain. The reason lies in the fact that these functions treat the TF plane as two separate spaces [2]. However, Hermite window functions, with their advantageous properties, can be used to consider the joint TF domain. Namely, these window functions are localized in TF domain, i.e. optimally localized in the circular TF region: $(t,f): t^2 + f^2 \le R^2$, of area πR^2 [10]. Therefore, the family of Hermite functions can be defined as follows [13,32]:

$$h_k(t) = \frac{1}{||H_k||} H_k(t) \sqrt{w(t)}, \quad k \in \mathbb{N} \tag{6}$$

where k denotes the order of the Hermite function ($k = 0, 1, \ldots, K$), $w(t) = e^{-t^2}$ is the Hermite weight function and $||H_k||$ is a normalization factor. Namely, it is necessary to normalize the Hermite polynomial function $H_k(t)$ to avoid ill-conditioned numerical computations [7].

It is well known that the classical orthogonal polynomials obey a three-term recurrence relation, which can be used to evaluate the corresponding Hermite functions:

$$h_k(t) = t\sqrt{\frac{2}{k}} h_{k-1}(t) - \sqrt{\frac{k-1}{k}} h_{k-2}(t), \quad k \ge 2, \tag{7}$$

where the initial terms are

$$h_0(t) = \frac{1}{\sqrt[4]{\pi}} e^{\frac{-t^2}{2}}, \qquad h_1(t) = \frac{\sqrt{2}t}{\sqrt[4]{\pi}} e^{\frac{-t^2}{2}}. \tag{8}$$

The first few Hermite polynomials with the corresponding Hermite functions are shown in Fig. 1. It can be seen that the zero-order Hermite function $h_0(t)$ (given by eq. (8)) corresponds to the Gaussian window function. Also, $h_k(t)$ (given by eq. (7)) quickly tends to zero as $|t|$ tends to infinity, thus $h_k's$ are assumed to be compactly supported functions. In practice, this is a very useful property since the computations involving Hermite functions can be reduced to a finite number of points within the effective support. The computation of the Hermite-Fourier coefficients $\langle x, h_k \rangle$ is a typical example where the integral over $[-\infty, \infty]$ can be approximated very well by applying numerical quadrature rules within the effective support. In our implementation, we used the composite trapezoidal rule with N points to evaluate the Hermite-Fourier coefficients $\langle x, h_k \rangle$ of a signal x with N number of samples.

The derivatives of Hermite functions can also be calculated recursively:

$$\frac{\partial h_k}{\partial t} = \sqrt{2k} h_{k-1} - t h_k, \quad k \ge 0, \tag{9}$$

and the set $\{h_k : k \in \mathbb{N}\}$ of functions forms an orthonormal and complete system in $L^2(\mathbb{R})$ with respect to the usual dot product and the norm [32]:

$$\langle h_k, h_\ell \rangle = \int_{-\infty}^{\infty} h_k(t) h_\ell(t) \mathrm{d}t = \delta_{k\ell}, \quad \|h_k\| := \sqrt{\langle h_k, h_k \rangle}, \tag{10}$$

where $\delta_{k\ell}$ stands for the Kronecker delta symbol.

The weight coefficients $d_k(t)$ in eq. (4) are calculated to satisfy IF constraints versus various polynomial phase orders K according to [8]:

$$\sum_{k=0}^{K-1} d_k(t) M_n^k(t) = \begin{cases} 1, & n = 0 \\ 0, & n > 0 \end{cases} \quad (n = 0, 1, \ldots, K-1), \tag{11}$$

where $M_n^k(t)$ is n-th order moment of the spectrogram $S_k(t,\omega)$ given for a signal of amplitude $A(t)$ as follows:

$$M_n^k(t) = \frac{\int A^2(t+\tau) h_k^2(\tau) \tau^n \, d\tau}{\int A^2(t+\tau) h_k^2(\tau) \, d\tau} \quad (n = 0, 1, \ldots, K-1). \tag{12}$$

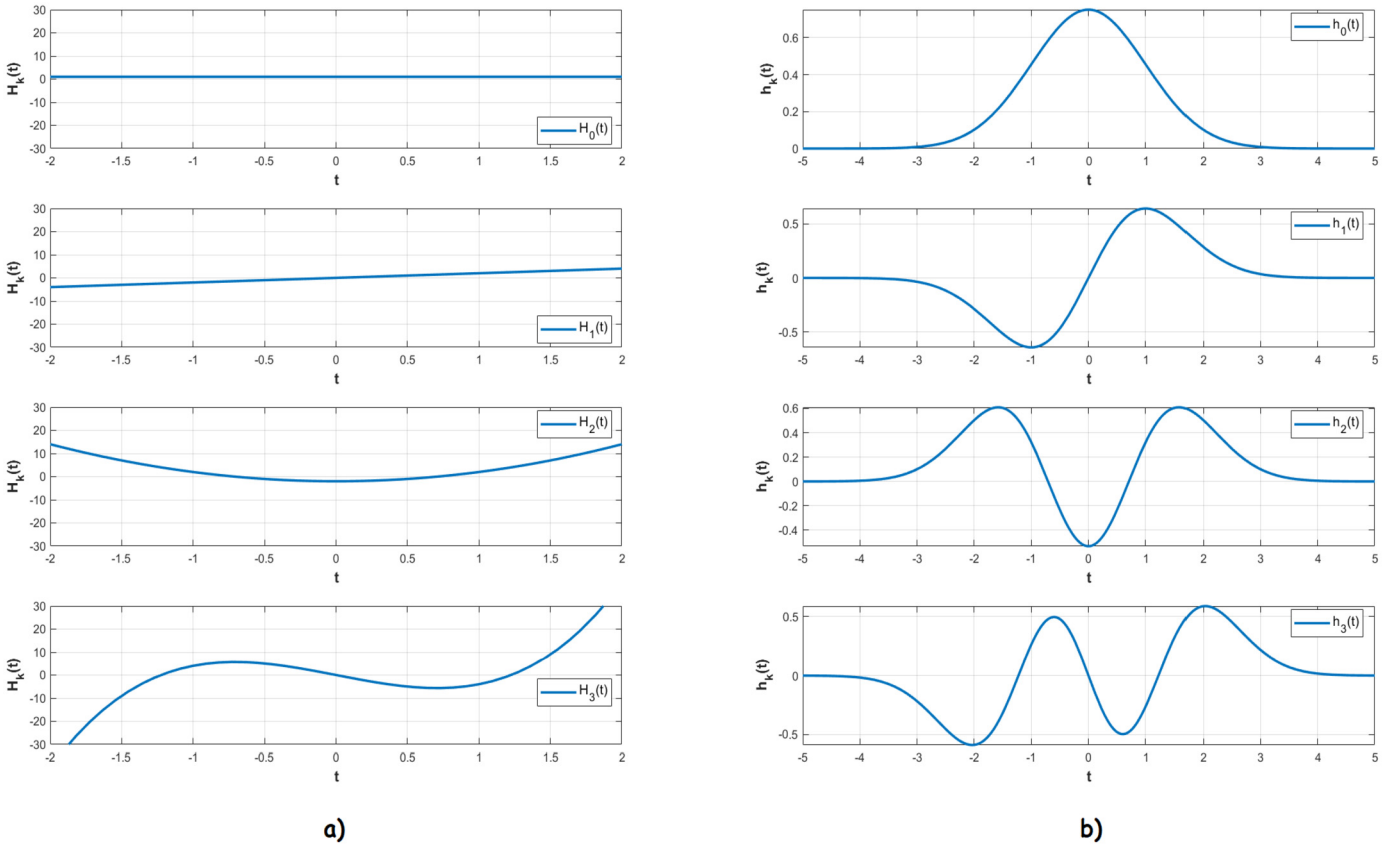

Fig. 1. a) Orthogonal Hermite polynomials with corresponding b) Hermite functions for the first few orders ($k = 0, 1, 2, 3$).

Therefore, the appropriate weight coefficients are computed with K Hermite window functions and by solving a set of equations given in eq. (11) with K spectral moments for each window function $h_k(t)$. The computation of the weight coefficients can be performed in matrix form using an appropriate regularization procedure. In doing so, the complexity of the computation can be costly.

Note that for constant or slowly varying amplitude signals ($A(t+\tau) = A(t)$), the weighting coefficients $d_k(t)$ have constant values. In this case, all odd-order moments M^k_{2n-1} have zero value and $h_k(t)^2$ is an even function of time. Therefore, the computation of the optimal coefficients is performed only for even-order moments, reducing the number of optimal windows in eq. (11). A precomputed weighting coefficients values d_k for constant or slowly varying amplitude signals, up to tenth order, can be found in [23]. These constant values can be used in cases where the matrix of moments is ill-conditioned to initialize the regularization process described in the following section.

3. Parameterized multiple window spectrogram

By including free parameters in the system of Hermite functions, the Hermite system can be defined as follows:

$$h_k^{\gamma,\lambda}(t) = \sqrt{\lambda} h_k(\lambda(t-\gamma)) \qquad (t, \gamma \in \mathbb{R}, \lambda > 0), \tag{13}$$

where γ and λ stand for the translation and the dilatation parameters, respectively. Fig. 2 shows an example of how these parameters affect the shapes of the parameterized Hermite basis functions. The dilatation parameter λ scales the unit on the real axis, while the translation γ shifts the central point in the time domain. In other words, λ controls the localization in the frequency domain, while γ localizes the signal components in the time domain. The smaller the value of the dilatation parameter, the larger the window width (i.e., the length of the effective support of $h_k^{\gamma,\lambda}$). The purpose of γ is less obvious since a uniform time shift is naturally performed in the spectrogram via windowing. However, our approach differs to a great extent from the common MW distributions since the time shifts are not distributed uniformly through the whole data due to the independent translation of the Hermite window functions in each signal segment. The proper choice of γ gives an additional degree of freedom to include or exclude some parts of the data in the spectral estimate, which is demonstrated in Fig. 3b. The dashed magenta rectangles indicate those parts of the signal that are suppressed by the tails of the Hermite window functions; therefore, they would be excluded from the final spectral estimate.

From a mathematical point of view, the linear parameterization $\lambda(t-\gamma)$ of the Hermite functions has several advantages. First, it can be shown that the new function system $\{h_k^{\gamma,\lambda} : k \in \mathbb{N}\}$ preserves orthonormality and completeness for all $0 < \lambda$ and $\gamma \in \mathbb{R}$. Second, the partial derivatives can be easily computed by the chain rule:

$$\frac{\partial h_k^{\gamma,\lambda}}{\partial \gamma} = -\lambda\sqrt{\lambda} \left.\frac{\partial h_k}{\partial t}\right|_{t=\lambda(t-\gamma)} \tag{14}$$

and

$$\frac{\partial h_k^{\gamma,\lambda}}{\partial \lambda} = \frac{1}{2\sqrt{\lambda}} h_k^{\gamma,\lambda} + (t-\gamma)\sqrt{\lambda} \left.\frac{\partial h_k}{\partial t}\right|_{t=\lambda(t-\gamma)}, \tag{15}$$

where the derivatives of the classical Hermite functions $\partial h_k/\partial t$'s are given in eq. (9). This allows the use of gradient-based optimization techniques in finding the best values for γ and λ.

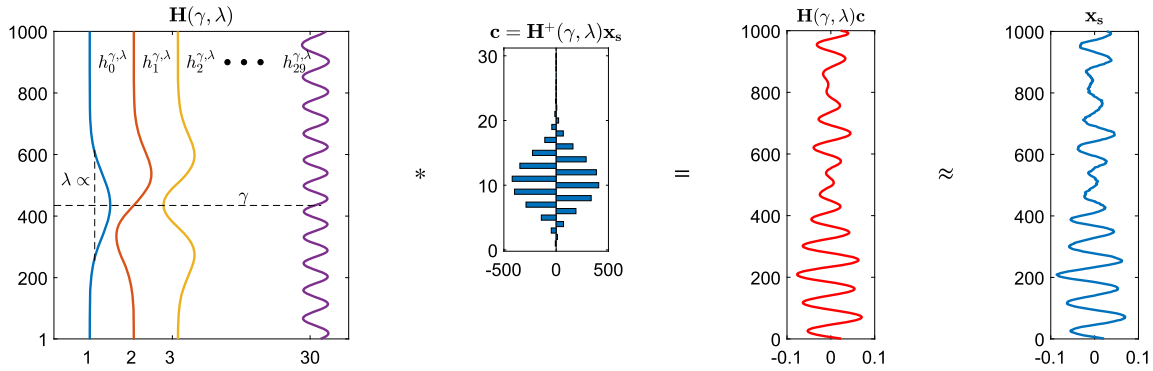

Fig. 2. Demonstrating the elements of the VP-functional for γ =434.6 and $\lambda = 0.001$: The matrix of parameterized Hermite functions $\mathbf{H}(\gamma, \lambda)$, the ordinary least squares solution $\mathbf{c} = \mathbf{H}^{+}(\gamma, \lambda)\mathbf{x_s}$, and the least squares approximation $\mathbf{H}(\gamma, \lambda)\mathbf{c}$ of the original signal segment $\mathbf{x_s}$.

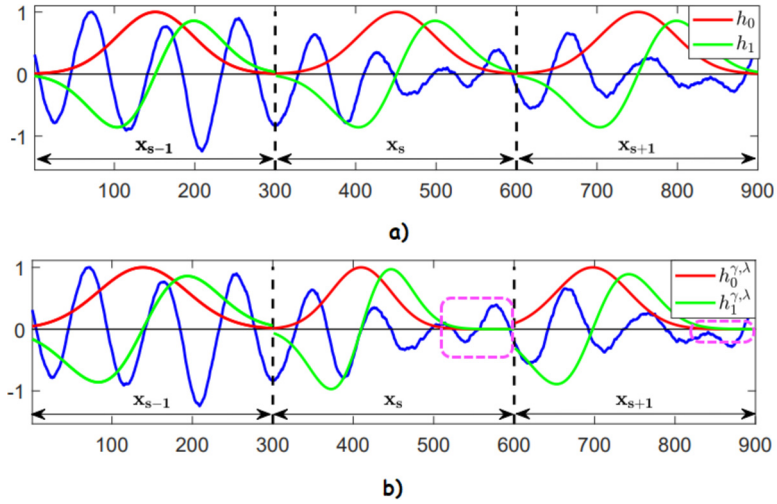

Fig. 3. Demonstrating the effect of multiple windows by using *a)* fixed and *b)* adaptive Hermite functions without overlap. (For interpretation of the colors in the figure(s), the reader is referred to the web version of this article.)

Here we propose a MWS approach where the window functions $h_k^{\gamma,\lambda}$ vary over time. Namely, in each signal segment $\mathbf{x_s} = [x(t), x(t+T), \ldots, x(t+(L-1)T)]^T$ of length L and sampling frequency $1/T$, the optimal values of γ and λ are determined by minimizing the VP-functional [11]:

$$r_2(\gamma, \lambda) := \left\| \mathbf{s} - \mathbf{H}(\gamma, \lambda)\mathbf{H}^{+}(\gamma, \lambda)\mathbf{s} \right\|_2^2, \tag{16}$$

where the k-th column of the matrix $\mathbf{H}(\gamma, \lambda) \in \mathbb{R}^{L \times K}$ represents $h_k^{\gamma,\lambda}(t)$ sampled at $t = 0, 1, \ldots, L-1$, and $\mathbf{H}^{+}(\gamma, \lambda)$ represents the Moore–Penrose pseudoinverse of $\mathbf{H}(\gamma, \lambda)$.

Note that the window length and hop size are hyperparameters of each TF distribution method, and their values are preset before the STFT calculations. Due to the discrete nature of these hyperparameters, their optimal values are typically determined via an exhaustive grid search. In our approach, these hyperparameters are assumed to be continuous variables, and hence their optimal values are determined by minimizing the VP-functional in eq. (16). In this way, it is enough to provide a rough initial estimate of the window length and the hop size, which are refined in each signal segment. Fig. 3 demonstrates this process, where the uniform time and frequency resolutions in Fig. 3a are rescaled non-uniformly in Fig. 3b. We note that the center of the Hermite windows γ and their length λ could be optimized simultaneously for each segment $\mathbf{x_s}$ to take into account the influence of neighboring segments. However, this would be computationally expensive, so we consider segment-wise optimization of γ and λ.

3.1. Optimization methods

We have implemented two different optimization methods, with and without gradient information. The first one provides unconstrained nonlinear optimization using the Nelder–Mead simplex algorithm and does not require information about the gradient of the error function. Another one is defined as extensions of Newton's method with the analytical gradient in each step. It performs nonlinear constrained optimization and supports linear and nonlinear constraints. The minimization of the VP-functional in eq. (16) is a separable nonlinear least-squares problem for which the gradient can be computed simply based on the partial derivatives of the basis functions [21]. It should be noted that all nonlinear optimization methods require decent initial parameters, mainly to avoid the local minimum problem. The proper initial parameter was determined based on experiments. Fig. 4 shows an approximation before and after parameters optimization of the Hermite functions, with the corresponding Hermite-Fourier power spectra.

A wide range of smooth functions can be used for windowing. However, it is desirable to reduce the signal samples to zero at the end of the window segment. An arbitrary parametrization of the Hermite functions does not necessarily satisfy these constraints; thus, the windowed signal segment can have a discontinuity at the borders. In order to avoid this phenomenon, we design nonlinear constraints which keep the parameters of the Hermite functions in a feasible region. We begin with the zero-order Hermite function $h_0(t)$, which is equal, up to a constant factor, to the probabil-

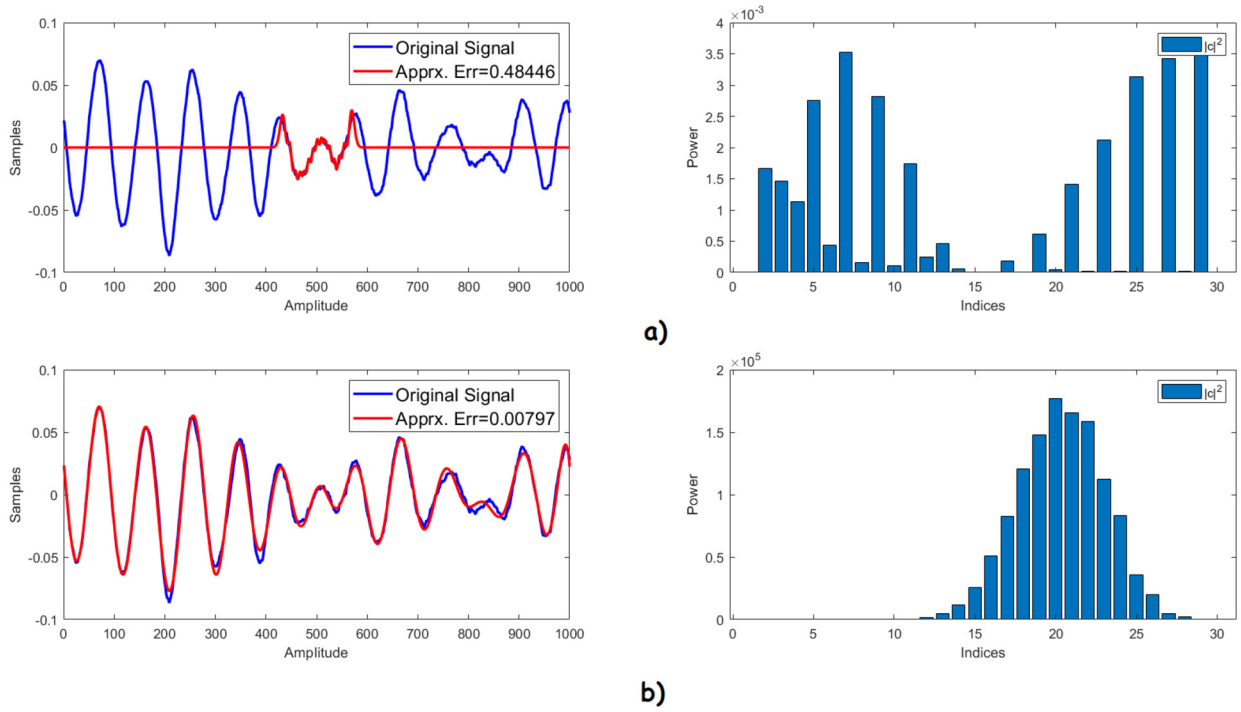

Fig. 4. Example of approximations by the Hermite Functions with corresponding Hermite-Fourier power spectra before a) and after b) optimization procedure.

ity density function of the standard normal distribution. By the so-called three-sigma rule, 99% of the overall integration of $h_0(t)$ lies within three standard deviations away from the mean, that is $[-3, 3]$. Outside this interval, $h_0(t)$ is negligibly small. A proper discretization of h_0 must preserve this property, thus we choose the sampling interval $[a, b]$ such that $[-3; 3] \subset [a; b]$ holds. For instance, in Fig. 1, we set $[a; b] = [-5; 5]$. The parametrization we proposed in Section 3 changes the sampling interval, we claim, however, that the property $[-3, 3] \subset [\lambda(a-\gamma), \lambda(b-\gamma)]$ must hold. This way, the optimization of γ and λ can be restricted to the feasible set:

$$\Gamma = \left\{ (\gamma, \lambda) \in \mathbb{R} \times \mathbb{R}_+ \,:\, \gamma + \frac{3}{\lambda} \leq b, \quad \gamma - \frac{3}{\lambda} \geq a \right\}. \tag{17}$$

Similar constraints can be derived for higher-order Hermite functions by using the fact that the effective support of h_j increases with the degree j. Indeed, the effective support of h_j is nested into the effective support of h_{j+1}; thus, it is enough to provide an estimation for the Hermite function with the highest degree, and then adjust the constraints accordingly. For instance, in the case of $K = 30$, we found that $[-9, 9]$ is a good estimate for the effective support of h_{29}, thus 3 can be replaced with 9 in eq. (17). Fig. 5 shows a typical example of how the nonlinear parameters γ and λ influence the condition number of the matrix $\mathbf{H}$. Note that the y-axis is scaled up by 10^7 due to the ill-conditioned examples (red and blue curves), whereas the feasible examples (black dashed curve) always result in a condition number equal to 1.

Besides numerical stability, orthogonality is another property that might be lost after discretization. There are uniform and non-uniform sampling methods to treat this issue [32]. For instance, the Gaussian quadrature rule is a classical non-uniform sampling method to construct discrete orthogonal function systems. In this approach, the first K Hermite functions h_k, $k = 0, \ldots, K-1$ are sampled over the roots of the $(K+1)$th Hermite function h_K. Although there is no explicit formula to calculate these roots, they can be precomputed. Then the corresponding sampling points of the parameterized Hermite functions $h_k^{\gamma,\lambda}$ can be derived by inverting the linear argument transform we proposed in eq. (13). Namely, if t_k denotes the roots of h_k, then the corresponding roots of $h_k^{\gamma,\lambda}$ are expressed as $t_k/\lambda + \gamma$. The precomputation of the roots can be done offline (i.e., once in a lifetime), whereas the transformation of these roots along with the non-uniform resampling of the input signal must be recomputed multiple times during the optimization. The extra computational cost caused by the resampling of the input signal can be avoided via uniform sampling, which is another discretization approach. Although it is well-known that the Hermite functions lose orthogonality over uniform sampling grids, we found that near-orthogonality of the function system $\{h_k^{\gamma,\lambda} : k = 0, \ldots, K-1\}$ can be maintained, provided that the number of sampling points is large enough ($L > 100$), and $(\gamma, \lambda) \in \Gamma$. An example is shown in Fig. 5, where we plotted the Frobenius norm of the non-diagonal entries of $\mathbf{H}^T(\gamma, \lambda)\mathbf{H}(\gamma, \lambda)$. Indeed, the product resembles to an identity matrix (i.e., $\langle h_i^{\gamma,\lambda}, h_j^{\gamma,\lambda} \rangle = \delta_{ij}$) when the nonlinear parameters γ and λ are chosen from the feasible set Γ.

3.2. Regularization techniques

After the optimization, the next step is to combine the Hermite window functions such that the IF constraints are satisfied [8]. To this end, the system of linear equations $\mathbf{Md} = \mathbf{b}$ must be solved, where M_{ij} is the i-th moment of the j-th Hermite window, and $\mathbf{b} = [1, 0, \ldots, 0]^T$ according to eqs. (11)-(12). Typically, $\mathbf{M}$ is a highly ill-conditioned matrix, which makes the solution very sensitive to perturbations of $\mathbf{M}$ and $\mathbf{b}$. Although the numerical representation of $\mathbf{b}$ is exact (contains only zeros and ones), the elements of $\mathbf{M}$ are just approximations to the true spectral moments due to the discretization of the integral in eq. (12). In addition to the discretization error, the numerical solvers involve round-off errors accumulating at the end of the calculations and dominating the solution. Thus, standard algorithms (e.g., LU, Cholesky, QR factorization) cannot be applied to get a meaningful solution; more sophisticated numerical regularization methods must be used instead. There are

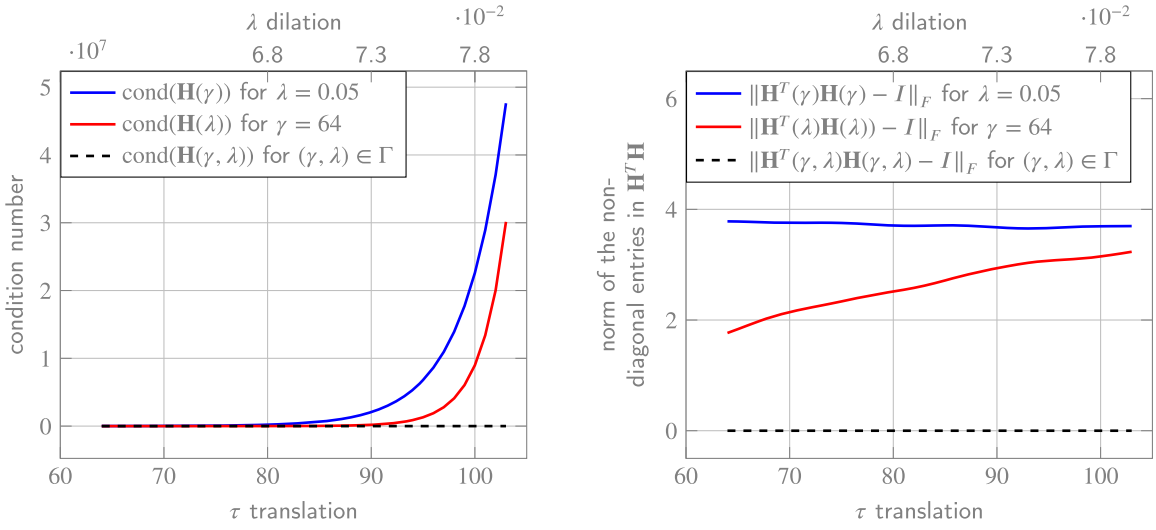

Fig. 5. Influence of γ, λ on the numerical properties of the matrix $\mathbf{H}(\gamma, \lambda) \in \mathbb{R}^{L \times K}$. Left: connection between the nonlinear parameters γ, λ and cond($\mathbf{H}(\gamma, \lambda)$) for $L = 128$ and $K = 20$. Right: orthogonality of the columns of $\mathbf{H}(\gamma, \lambda)$ for various parameter setups.

various ways to formalize the regularization; among them, the penalized least-squares method is a common technique to solve ill-conditioned problems:

$$\widetilde{\mathbf{d}}_\beta = \arg\min_{\mathbf{d}} \{\|\mathbf{b} - \mathbf{M}\mathbf{d}\|_2^2 + \beta^2 \Omega(\mathbf{d})\}, \tag{18}$$

where $\beta > 0$ stands for the regularization parameter, and $\Omega(.)$ is a penalty function. For instance, $\Omega(\mathbf{d}) = \|\mathbf{d}\|_p$ for $p = 1, 2$ is a typical choice for the penalty term that allows to regulate mathematical properties of the solution $\mathbf{d}$, such as smoothness, non-negativity, and sparsity. In our experiments, we tested several professional numerical solvers, such as Tikhonov regularization, truncated and damped singular value decompositions from RegTool [16], and the *IRhybrid_lsqr* and the *IRell1* MATLAB routines from the IRTool [14] package.

In eq. (18), β is a crucial parameter, which controls the tradeoff between under- and over-fitting. Searching for the optimal value of β is a demanding problem, but various heuristics, such as cross-validation, normalized cumulative periodogram, L-curve [15], exist to estimate it. In our experiments, we utilized the L-curve method, which is one of the most intuitive model-selection approaches. Namely, if we plot the residual norm $\|\mathbf{b} - \mathbf{M}\widetilde{\mathbf{d}}_\beta\|_2$ versus the norm of the regularized solution $\Omega(\widetilde{\mathbf{d}}_\beta) = \|\widetilde{\mathbf{d}}_\beta\|_2$ in a log-log scale for several values of β, the resulting curve will resemble to the letter L whose corner point is a good estimate of the optimal value of β. Note that this method requires the evaluation of the L-curve at several points, i.e., eq. (18) must be solved for several values of β; hence, this method is appropriate for small-scale problems only. However, the computational effort required to calculate the L-curve is negligible compared to the regularization method since the size of the matrix $\mathbf{M}$ is proportional to the number of Hermite window functions K, which is typically small (< 100).

4. Experimental results

The efficiency of the proposed parameterized MWS method is tested and discussed in this section. Through detailed experimental analysis, the achieved performances are compared to other competitive TFD methods. Namely, we compared the simulation results obtained by the raw spectrogram, WVD, raw MWS, and proposed parametrized MWS methods for a set of mono- and multi-component, synthetic, slowly-varying, non-stationary noisy signals. To confirm the efficiency of the proposed method, we assessed performances of parametrized MWS in terms of the IF estimation accuracy, TF concentration, and improvement in TF representation. The IF estimation accuracy is evaluated by the MSE averaged over a number of iterations to confirm the estimation accuracy improvement and to guarantee that the proposed MWS method provides TF representation suitable for IF estimation. For evaluating the signal information content and the TF representation in the TF plane, we employ the Rényi entropy as a quantitative concentration measure [1,4]. Additionally, the proposed MWS method is applied to examples of real-world ship motion data to demonstrate performance improvement in practical scenarios.

4.1. Results for synthetic frequency modulated signals

The set of different synthetic frequency modulated signals is observed for the method's performance evaluation, such as linear frequency modulated (LFM) and parabolic frequency modulated (PFM) mono-component signals, as well as a multi-component signal with sinusoidal frequency modulation (SFM). IF estimation accuracy is analyzed by MSE averaged over 100 realizations of randomly generated additive, white, Gaussian noise with different SNR values. Nonlinear unconstrained and constrained optimization methods have been tested. It has been experimentally determined that it is most appropriate to use a programming solver that performs nonlinear constrained optimization and the analytical gradient in each step. Since this solver supports nonlinear constraints, we additionally tested the performance with designed nonlinear constraints. The initial free parameters in optimizers are experimentally determined for each SNR to avoid reaching the local minimum during optimization. Also, both optimizers are set to have the same number of iterations. Complete analysis and efficiency comparison, as well as the corresponding TF representations, are given below.

The LFM signal is considered with values of starting and ending normalized frequencies of 0.05 and 0.15, respectively, with 128 samples. The raw spectrogram with Hanning window, the WVD, the raw MWS, and the proposed parametrized MWS representations for the observed signal are shown in Fig. 6, with normalized TF magnitude values (rescaling the range of TF data to the interval $[0, 1]$). Raw MWS is calculated with 10 Hermite functions, experimentally determined to improve TF concentration and representation results. The proposed parametric approach is also computed with the same number of Hermite functions with a nonlinear optimization method. The initial values of dilatation λ

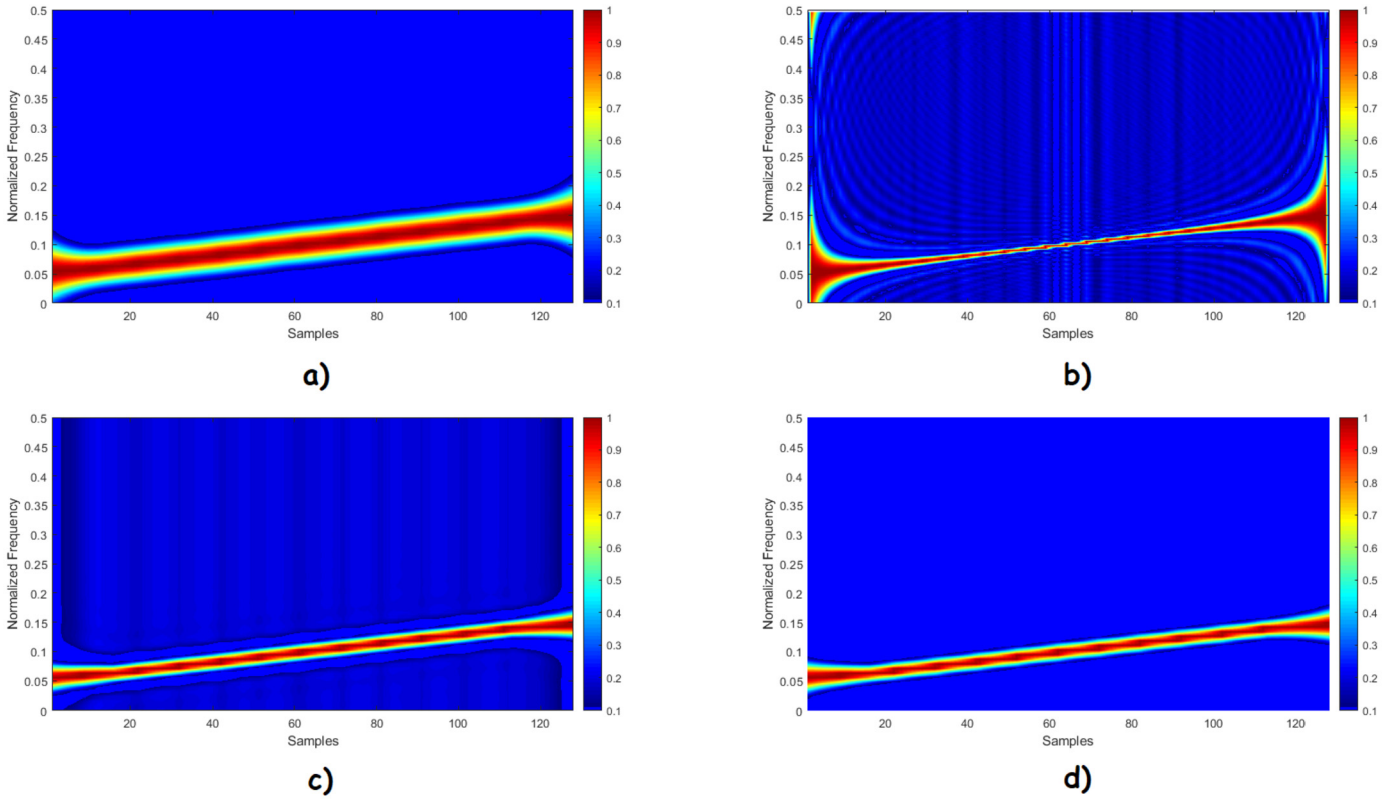

Fig. 6. TF representation of the LFM signal with SNR = 10 dB: a) Raw spectrogram, b) WVD c) Raw MWS ($K = 10$), d) Proposed parametrized MWS ($K = 10$).

and translation γ are determined experimentally to avoid the local minimum problem during optimization. Also, nonlinear constraints are designed to keep the parameters of the Hermite functions in a feasible region, as described in Section 3.1. One can see that the proposed parametrized approach significantly outperforms other representations for the tested noisy LFM signal.

Estimation of the IF was performed for different SNR values, and the mean values of MSE for 100 realizations of random noise are given in Table 1, for raw spectrogram, WVD, raw MWS, and for the proposed parameterized MWS distribution with and without nonlinear constraints. As expected, the accuracy of the IF estimation degrades with decreased SNR value for all presented distribution methods. However, the proposed method with designed nonlinear constraints provides significantly improved results compared to other TFDs, even for the noisy test scenarios with low SNR values. The raw MWS method is given here to compare and confirm the obtained improvement in the results. Namely, its efficiency can be improved by setting the appropriate parameters that are determined experimentally by a general grid search as explained in Section 3. On the other hand, the proposed parameterized method determines these values by minimizing the VP-functional given in eq. (16). Additionally, it should be noted that the best fitting initial values of the free parameters may vary in small quantities depending on the applied random noise. In the case of 100 test iterations, the best fitting initial values are set evenly for each iteration to, ultimately, obtain the minimum MSE.

The efficiency of the proposed method for a signal with PFM was tested in the same manner as for the LFM signal. We consider the signal $s(t) = e^{j2\pi(a_0 t + \frac{a_1}{2}t^2 + \frac{a_2}{3}t^3)}$, where a_0, a_1 and a_2 are coefficients of the polynomial instantaneous phase. To generate a signal with PFM law, we used a set of TF points in the form (t_i, f_i) as follows: $(1, 0.2)$, $(64, 0.05)$, $(128, 0.15)$. The coefficients a_0, a_1, and a_2 are then calculated to fit these points according to a PFM law. TF representation results for all analyzed distribution methods are given in Fig. 7. Averaged MSE values of the estimated IF obtained for 100 test iterations are given in Table 2. The proposed method with 11 parametrized Hermite functions and designed nonlinear constraints provides the best TF representation results for the tested PFM noisy signal compared to other competitive representations. Moreover, the proposed method is robust to noise. It should also be noted that the corresponding initial values of the free parameters need to be redefined and, hence, were adjusted experimentally.

Following experimental results for mono-component signals, we perform IF estimation efficiency tests for a multi-component signal consisting of two components having SFM. With the new initial values of the free parameters, the experimental results are given in Fig. 8. MSE values obtained for different SNR values are given individually, for each component, in Table 3. As it can be seen, the lowest mean MSE values for the estimated IF are ob-

Table 1
MSE of the IF estimation for different SNR values for the LFM signal ($\times 10^{-5}$).

TF Distribution	10 dB	7.5 dB	5 dB
Raw spectrogram	0.75	0.90	1.16
WVD	5.84	9.21	29.16
Raw MWS	0.73	0.84	0.96
Parametrized MWS without nonlinear constraints	0.79	0.86	0.99
Parametrized MWS with nonlinear constraints	**0.72**	**0.83**	**0.95**

Table 2
MSE of the IF estimation for different SNR values for the PFM signal ($\times 10^{-5}$).

TF Distribution	10 dB	7.5 dB	5 dB
Raw spectrogram	1.98	2.19	2.49
WVD	4.17	6.98	27.01
Raw MWS	1.75	2.12	2.31
Parametrized MWS without nonlinear constraints	1.31	1.57	1.95
Parametrized MWS with nonlinear constraints	**1.30**	**1.56**	**1.84**

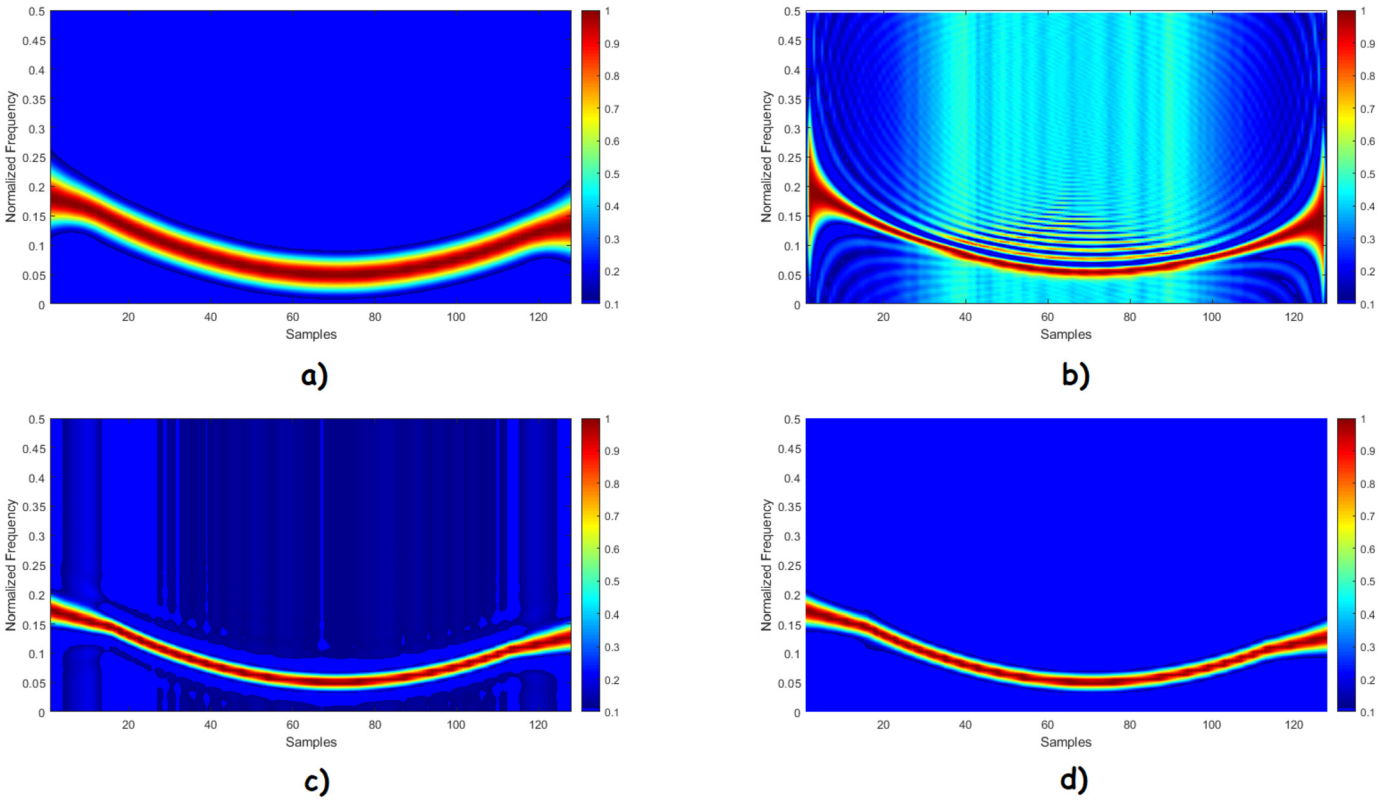

Fig. 7. TF representation of the PFM signal with SNR = 10 dB: a) Raw spectrogram, b) WVD c) Raw MWS ($K = 11$), d) Proposed parametrized MWS ($K = 11$).

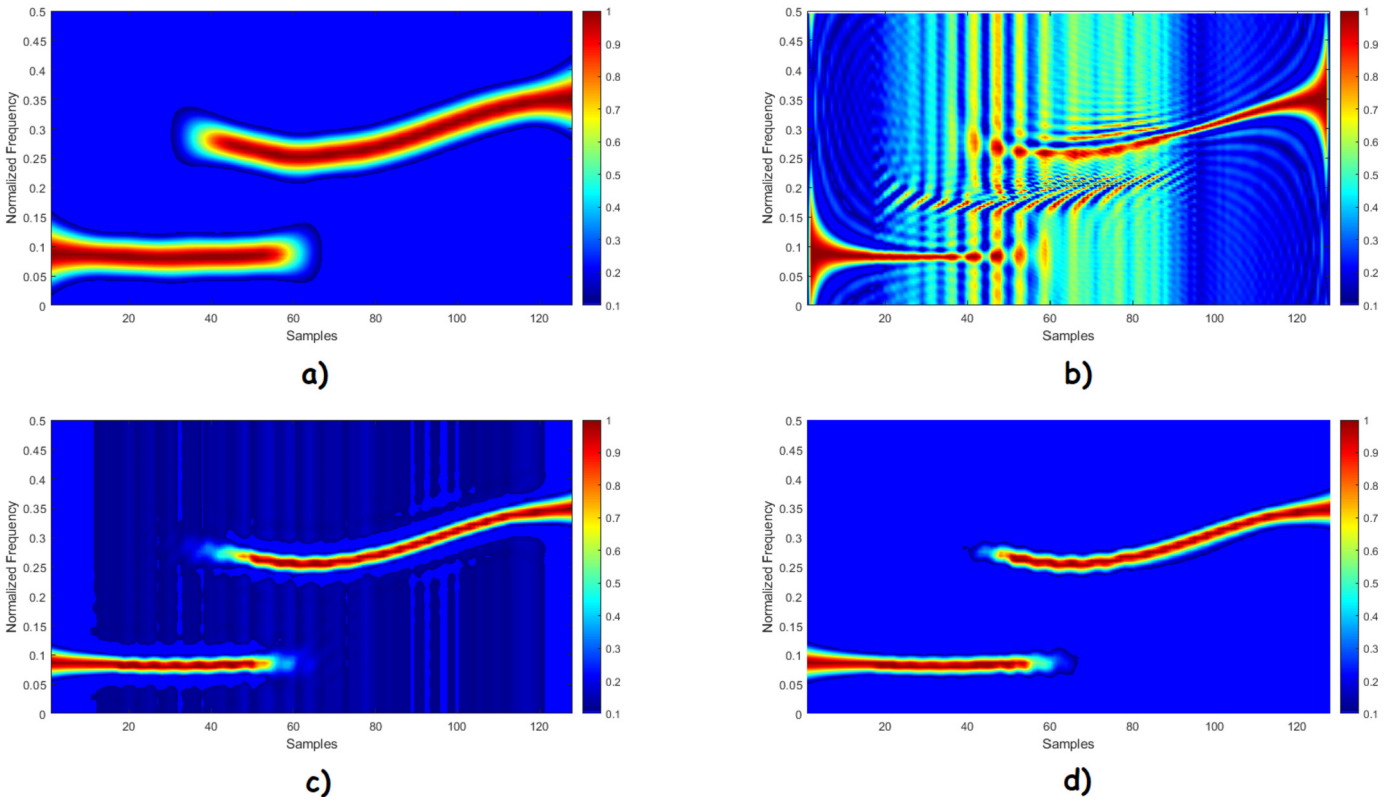

Fig. 8. TF representation of the multi-component SFM signal with SNR = 10 dB: a) Raw spectrogram, b) WVD c) Raw MWS ($K = 11$), d) Proposed parametrized MWS ($K = 11$).

Table 3
MSE of the IF estimation of each component for different SNR values for the multi-component SFM signal ($\times 10^{-5}$).

TF Distribution	10 dB Component 1 | Component 2	7.5 dB Component 1 | Component 2	5 dB Component 1 | Component 2
Raw spectrogram	0.36 | 11.72	0.41 | 26.68	0.44 | 39.19
WVD	7.76 | 2.53	7.71 | 6.25	7.62 | 14.46
Raw MWS	0.35 | 0.12	0.38 | 0.17	0.43 | 0.20
Parametrized MWS without nonlinear constraints	0.52 | 0.12	0.60 | 0.16	0.63 | 0.18
Parametrized MWS with nonlinear constraints	**0.29 | 0.10**	**0.33 | 0.15**	**0.36 | 0.17**

Table 4
TF concentration measured by the Renyi entropy for tested synthetic signals (SNR = 5 dB).

TF Distribution	LFM	PFM	SFM
Raw spectrogram	3.597	3.659	3.647
WVD	0.565	2.406	1.394
Raw MWS	0.358	0.447	0.436
Parametrized MWS without nonlinear constraints	0.515	0.527	0.416
Parametrized MWS with nonlinear constraints	**0.325**	**0.307**	**0.414**

tained by the proposed parametrized approach with applied nonlinear constraints.

The results show that the selected number and shape of the Hermite window functions can be of great importance for obtaining improved performance results. The proposed method achieves improved results with a small number of functions and outperforms the competitive ones for both mono- and multi-component frequency-modulated noisy signals. Due to the smaller number of Hermite functions being sufficient for the proposed method, the computation time for the calculation of weight coefficients in eq. (11) is similar to that in the raw MWS method. Hence, we can conclude that the proposed parameterized MWS method is robust to noise and gives favorable results in terms of TF representation and IF estimation accuracy.

To additional evaluate the performances of the proposed method in terms of TFD concentration, we utilize the Rényi entropy measure of order 3. Results of the Rényi entropy obtained for different TFDs are given in Table 4. As it can be seen, the entropy values are reduced using the proposed MW approach, and, ultimately, the proposed parameterized method results in a more concentrated TFD outperforming the tested competitive methods.

4.2. Results for real-world ship motion response signals

Maintaining stable operational performance for ship routing in rough weather conditions and/or restricted navigation areas is of great importance for safety and navigational efficiency (in terms of fuel consumption and greenhouse gas emissions). In such conditions, it is appropriate to use on-board Decision Support Systems (DSS) that help operators make more precise control decisions, providing them with information on essential data [28]. DSS consists of many different modules and algorithms to analyze and filter measured motion responses and contribute to advanced sea state estimation techniques associated with the Directional Wave Spectra (DWS). Recently, the common DWS estimation technique follows the idea of wave buoy analogy. It represents a more efficient alternative to moored buoys, satellite, and radar measurements, as it aims to measure only available ship responses from different ship sensor systems, thus achieving less complexity, simpler maintenance, and ultimately lower costs [20]. The DWS estimation with wave buoy analogy has different formulations, and most of them are given in the frequency domain with the assumption of linearity between the measured motion response spectra and the DWS:

$$S_{ij}(\omega_e) = \int_{-\pi}^{\pi} H_i(\omega_e,\theta)\overline{H_j(\omega_e,\theta)}E(\omega_e,\theta)d\theta, \tag{19}$$

where $S_{ij}(\omega_e)$ denotes the response spectrum of the ship's motion and $E(\omega_e,\theta)$ denotes the corresponding DWS for the encounter frequency ω_e and angle θ. Their relationship is given with the prior knowledge of the ship behavior under certain wave conditions, which are described with complex transfer functions, called response amplitude operators (RAO), denoted as H_i and H_j. Estimation accuracy and trustworthiness depend mainly on the reliability of the RAO functions and/or the performance of the spectral analysis. Since the accuracy of the RAO may be insufficient due to the incomplete knowledge of the input conditions, it is of great importance to recognize the possibility of improvement by suitable filtering and processing algorithms with analysis in the TF domain. Thus, the contribution to the effectiveness of such systems depends significantly on the integrated modules for advanced signal processing.

While routing, the ship encounters stochastic environmental forces (such as waves, wind, and sea currents), and response signals introduce interferences into the system. Consequently, the acquired noisy signals need to be processed before being passed to the control algorithm. Thus, we observed noisy non-stationary signals modeled as random, non-stationary processes with time-varying spectral content. Indeed, it is possible to observe the response spectra for six degrees of ship motions (pitch, roll, heave, sway, surge, and yaw). The most commonly used motions are the pitch, roll, and heave motions with their couplings. Those motions are mainly caused by the sea waves and are least affected by the operation of the thrusters.

Considering the favorable properties of the proposed parametrized MWS approach, we perform the analysis of the spectral content of real-world ship motion response signals and demonstrate the efficiency of the proposed parametrized method with examples of ship navigation data. We selected ship motion response signals (in multiple degrees of freedom) from a dataset observed within rough sea navigation in 2013 in the Southern Hemisphere. Data length is one hour in each subset of the dataset with a time interval of 0.1 seconds. The observed 20,000DWT Bulk Carrier ship has a length of 160.4 m and a width of 27.2 m. For example, we used pitch motion response signals in two scenarios, usual ship navigation and navigation with speed loss due to the influence of environmental forces. For the observed noisy motion response signals (with a low frequency), the intention was to produce the best possible TF concentration with minimized variance and high-concentration TF representation using parametrized Hermite functions.

For the proposed parameterized MWS method, in all cases, the initial values of the free parameters were set to $\lambda = 20/N$ and $\gamma = N/2$, where N is the number of samples. Applied nonlinear optimizer with gradient information is set with a maximum of 30 allowed iterations. The number of Hermite functions K was determined experimentally to achieve the best performance.

Fig. 9 shows examples of pitch motion signals (with and without speed loss) in the time domain, demonstrating performances of Hermite expansion using a programming solver which performs

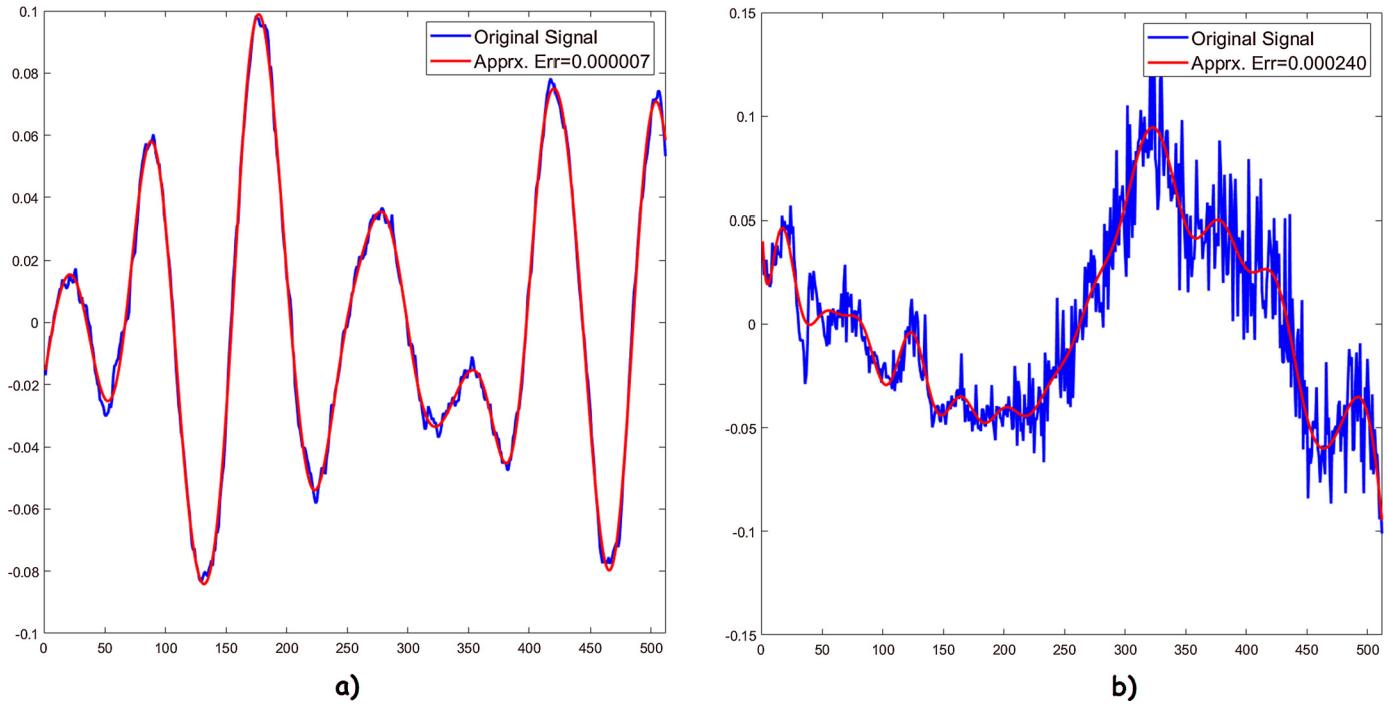

Fig. 9. An example of ship motion signal and the corresponding Hermite expansion for an a) Pitch motion and b) Pitch motion in speed loss cases.

Table 5
TF concentration measured by the Renyi entropy for tested real-world ship pitch motion response signals.

TF Distribution	Pitch Motion without Speed Loss	Pitch Motion with Speed Loss
Raw spectrogram	3.37	3.77
WVD	1.09	2.03
Raw MWS	0.86	0.68
Parametrized MWS	0.77	0.44

nonlinear constrained optimization with designed nonlinear constraints. The obtained MSE of the VP-approximation is rather low, with values $\text{MSE} = 6.57 \cdot 10^{-6}$ for the normal navigation case and $\text{MSE} = 2.40 \cdot 10^{-4}$ for the speed loss case. With such small values of the approximation error, optimal values of free parameters were obtained. These values are further used to calculate the parameterized Hermite functions according to the eq. (13) as a part of the MWS calculation procedure.

The TF representation results are given in Fig. 10 for usual pitch motion response, while Figs. 11 and 12 show two examples of pitch motion responses in the case of speed loss. In this way, achieved improved ship motion response data representation in the TF domain is clearly demonstrated. Additionally, compared to other analyzed methods, the proposed method with parameterized Hermite functions and applied nonlinear constraints provides the lowest Rényi entropy values, thus representing the most concentrated TFD (see Table 5). Given the results obtained, we can conclude that the proposed method effectively analyzes real-life ship motions signals and outperforms other competitive distribution approaches in terms of TF concentration enhancement and TF representation improvement.

It should be additionally noted, in the above example with speed loss, given in Fig. 12, the number of used Hermite functions has increased to achieve improved results. In our experiments, it turned out that $K = 30$ is appropriate to fit the windowed signal segments in the sense of eq. (20). Also, we found that $[-9, 9]$ is a good estimate for the effective support, as already described in 3.1. Due to the optimization, the Hermite spectra are centralized, and it turned out only 15 basis functions are enough, and the rest of the coefficients may be negligible. Therefore, the ship motion data can be represented in a very compact form using only 15 Hermite functions. However, when using a larger number of Hermite functions, as in this case, problems with round-off and discretization errors, as well as a highly ill-conditioned matrix, occur when solving $\mathbf{Md} = \mathbf{b}$. These problems have been mitigated successfully with the help of MATLAB routines from the IRTool package described in Section 3.2. Although the IRTool approaches are more computationally expensive compared to the other solvers we used, the proposed method results in significantly improved results.

To conclude, the given study shows that the proposed, novel parameterized MWS significantly outperforms the original MWS and other tested TFDs in terms of IF estimation accuracy and TF concentration. This was demonstrated on both synthetic and real-life signals.

5. Conclusion

With the proposed MWS method, a more suitable representation of the underlying features is obtained for various non-stationary frequency modulated signals. The optimization of nonlinear least-squares approximation of the response signals and parametrization of the Hermite functions lead to improved analysis results in terms of the TF concentration and accuracy of IF estimation. The proposed method also provides a reliable trade-off between minimized variance and stable bias estimates. Experimental results have shown that it outperforms other competitive non-adaptive and adaptive TFDs for both synthetic mono- and multi-component frequency modulated signals, as well as for tested real-world ship motion response signals. The improvement was achieved using only two free parameters and considered segment-wise optimization to lower the computational cost. In general, execution times are highly affected by regularization procedures when a larger number of Hermite functions are chosen, but increased execution times are neglectable in the case of a smaller number of Hermite functions. It has been shown that 15 basis functions are sufficient for representation and concentration improvement for

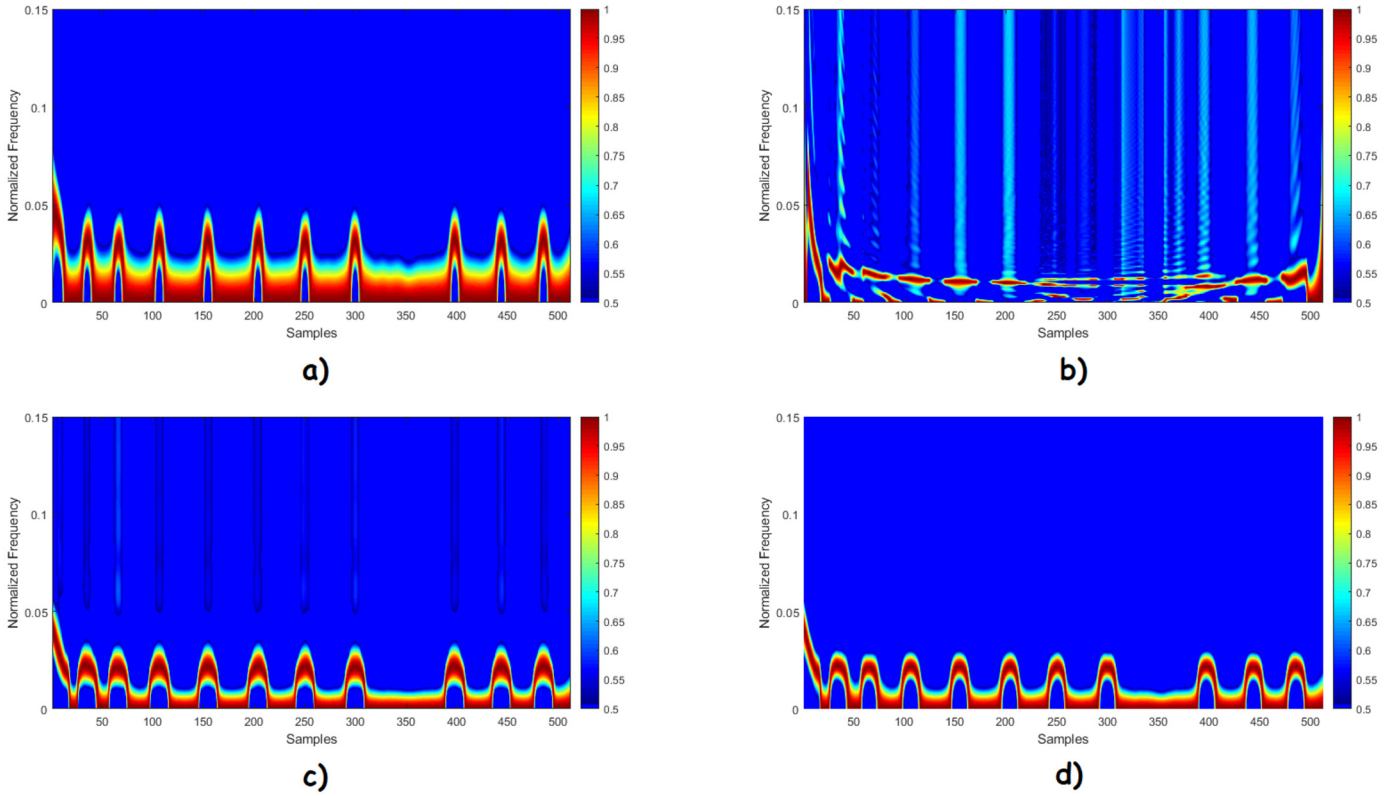

Fig. 10. TF representations of a ship pitch motion response signal: a) Raw spectrogram, b) WVD, c) Raw MWS ($K = 11$), d) Parametrized MWS ($K = 11$).

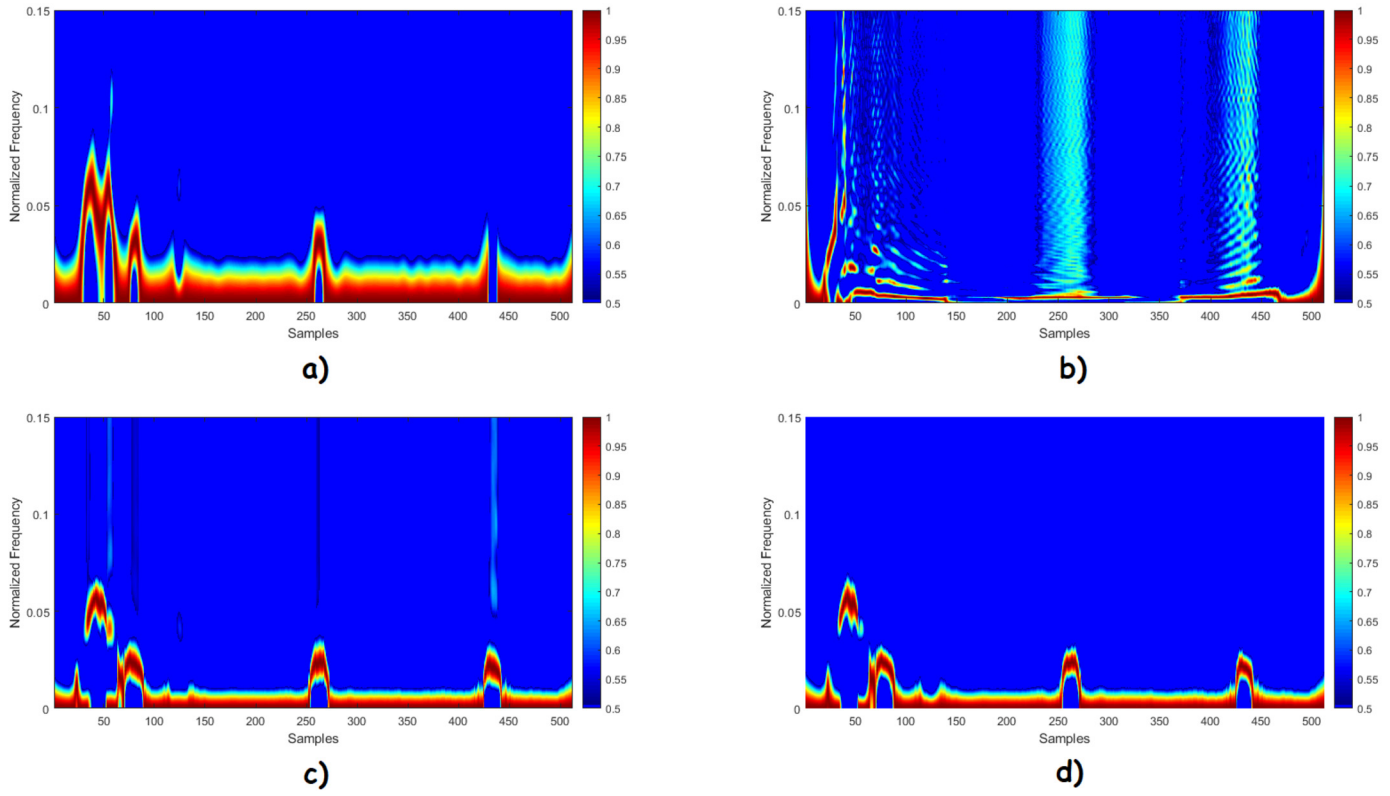

Fig. 11. TF representations of a ship pitch motion response signal with speed loss (example 1): a) Raw spectrogram, b) WVD, c) Raw MWS ($K = 11$), d) Parametrized MWS ($K = 11$).

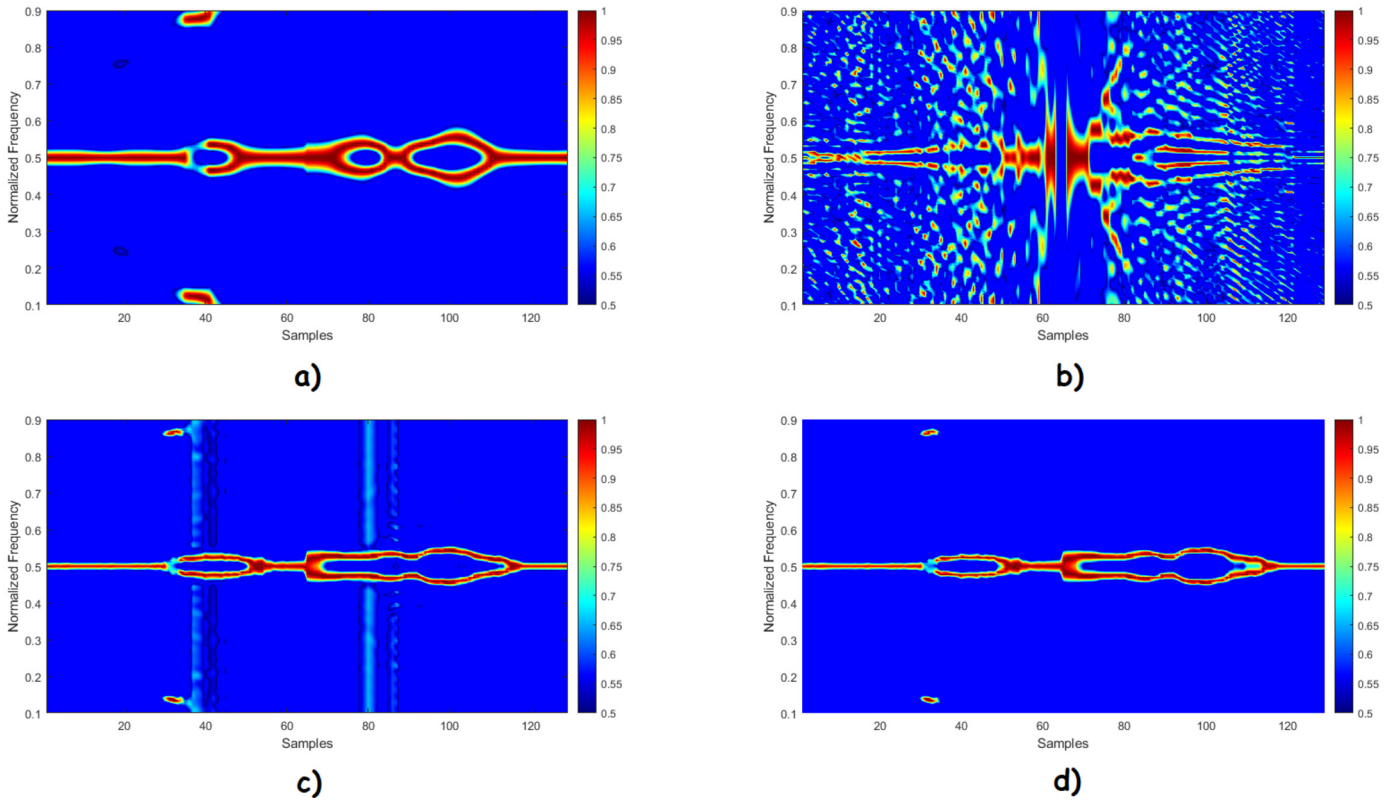

Fig. 12. TF representations of a ship pitch motion response signal with speed loss (example 2): a) Raw spectrogram, b) WVD, c) Raw MWS ($K = 11$), d) Parametrized MWS ($K = 30$).

ship pitch motion data. With additional modifications of the proposed MWS method, as modified weight coefficients, even better characteristics for spectral analysis can be expected. Since the free parameters in the MWS method need to be adaptively adjusted based on the applied noise, the application of machine learning algorithms for automatic parameters selection could be the next step to upgrade our future work.

CRediT authorship contribution statement

Denis Selimović: Investigation, Methodology, Software, Validation, Visualization, Writing – original draft. **Jonatan Lerga:** Conceptualization, Formal analysis, Funding acquisition, Investigation, Methodology, Project administration, Resources, Supervision, Validation, Writing – original draft, Writing – review & editing. **Péter Kovács:** Conceptualization, Investigation, Methodology, Software, Validation, Writing – original draft, Writing – review & editing. **Jasna Prpić-Oršić:** Conceptualization, Data curation, Formal analysis, Funding acquisition, Methodology, Project administration, Resources, Supervision, Validation, Writing – review & editing.

Declaration of competing interest

The authors declare that they have no known competing financial interests or personal relationships that could have appeared to influence the work reported in this paper.

Acknowledgment

This work was fully supported by the Croatian Science Foundation under the project IP-2018-01-3739, EU Horizon 2020 project "National Competence Centres in the Framework of EuroHPC (EUROCC)", IRI2 project "ABsistemDCiCloud" (KK.01.2.1.02.0179), University of Rijeka projects uniri-tehnic-18-17 and uniri-tehnic-18-15, Croatian–Slovenian bilateral project BI-HR/20-21-043, and the European COST project CA17137. Also, this paper was supported by the János Bolyai Research Scholarship of the Hungarian Academy of Sciences. Project no. TKP2021-NVA-29 has been implemented with the support provided by the Ministry of Innovation and Technology of Hungary from the National Research, Development and Innovation Fund, financed under the TKP2021-NVA funding scheme.

References

[1] R. Baraniuk, P. Flandrin, A. Janssen, O. Michel, Measuring time-frequency information content using the Renyi entropies, IEEE Trans. Inf. Theory 47 (2001) 1391–1409, https://doi.org/10.1109/18.923723.

[2] M. Bayram, R.G. Baraniuk, Multiple window time-frequency analysis, in: Proceedings of the IEEE-SP International Symposium on Time-Frequency and Time-Scale Analysis, Institute of Electrical and Electronics Engineers Inc., United States, 1996, pp. 173–176, Conference date: 18-06-1996 through 21-06-1996.

[3] B. Boashash, Advanced implementation and realization of TFDs, in: B. Boashash (Ed.), Time-Frequency Signal Analysis and Processing, second edition, Academic Press, Oxford, 2016, pp. 331–385, Chapter 6, http://www.sciencedirect.com/science/article/pii/B9780123984999000066, https://doi.org/10.1016/B978-0-12-398499-9.00006-6.

[4] B. Boashash, Measures, performance assessment, and enhancement of tfds, in: B. Boashash (Ed.), Time-Frequency Signal Analysis and Processing, second edition, Academic Press, Oxford, 2016, pp. 387–452, Chapter 7, https://www.sciencedirect.com/science/article/pii/B9780123984999000078, https://doi.org/10.1016/B978-0-12-398499-9.00007-8.

[5] C. Böck, P. Kovács, P. Laguna, J. Meier, M. Huemer, ECG beat representation and delineation by means of variable projection, IEEE Trans. Biomed. Eng. (2021) 1–12, https://doi.org/10.1109/TBME.2021.3058781.

[6] M. Boudiaf, M. Benkherrat, K. Mansouri, Denoising of single-trial event-related potentials using adaptive modelling, IET Signal Process. 11 (2017), https://doi.org/10.1049/iet-spr.2016.0528.

[7] J. Boyd, Dynamics of the equatorial ocean, https://doi.org/10.1007/978-3-662-55476-0, 2017.

[8] F. Cakrak, P.J. Loughlin, Multiwindow time-varying spectrum with instantaneous bandwidth and frequency constraints, IEEE Trans. Signal Process. 49 (2001) 1656–1666, https://doi.org/10.1109/78.934135.

[9] L. Cohen, The uncertainty principle for the short-time Fourier transform and wavelet transform, in: Wavelet Transforms and Time-Frequency Signal Analysis, Birkhäuser Boston, Boston, MA, 2001, pp. 217–232.
[10] I. Daubechies, Time-frequency localization operators: a geometric phase space approach, IEEE Trans. Inf. Theory 34 (1988) 605–612, https://doi.org/10.1109/18.9761.
[11] B. Fischer, G.H. Golub, How to generate unknown orthogonal polynomials out of known orthogonal polynomials, J. Comput. Appl. Math. 43 (1992) 99–115, https://core.ac.uk/download/pdf/82564792.pdf.
[12] G. Fraser, B. Boashash, Multiple window spectrogram and time-frequency distributions, in: IEEE International Conference on Acoustics, Speech, and Signal Processing, vol. 4, 1994, IV/293–IV/296, https://doi.org/10.1109/ICASSP.1994.389818.
[13] W. Gautschi, Orthogonal Polynomials, Computation and Approximation. Numerical Mathematics and Scientific Computation, Oxford University Press, Oxford, UK, 2004.
[14] S. Gazzola, P.C. Hansen, J.G. Nagy, IR tools: a MATLAB package of iterative regularization methods and large-scale test problems, Numer. Algorithms 81 (2019) 773–811.
[15] P.C. Hansen, Rank-Deficient and Discrete Ill-Posed Inverse Problems: Numerical Aspects of Linear Inversion, SIAM Monographs on Mathematical Modeling and Computation, SIAM, Philadelphia, PA, USA, 1998.
[16] P.C. Hansen, Regularization tools version 4.0 for Matlab 7.3, Numer. Algorithms 46 (2007) 189–194.
[17] M. Hansson, G. Salomonsson, A multiple window method for estimation of peaked spectra, IEEE Trans. Signal Process. 45 (1997) 778–781.
[18] P. Kovács, G. Bognár, C. Huber, M. Huemer, Vpnet: variable projection networks, Int. J. Neural Syst. (IJNS) 32 (2021) 2150054, https://doi.org/10.1142/S0129065721500544.
[19] P. Kovács, C. Böck, T. Dózsa, J. Meier, M. Huemer, Waveform modeling by adaptive weighted Hermite functions, in: 2019 IEEE International Conference on Acoustics, Speech and Signal Processing (ICASSP), ICASSP 2019, 2019, pp. 1080–1084.
[20] U.D. Nielsen, A concise account of techniques available for shipboard sea state estimation, Ocean Eng. 129 (2017) 352–362, https://www.sciencedirect.com/science/article/pii/S0029801816305388, https://doi.org/10.1016/j.oceaneng.2016.11.035.
[21] D.P. O'Leary, B.W. Rust, Variable projection for nonlinear least squares problems, Comput. Optim. Appl. 54 (2013) 579–593.
[22] I. Orovic, S. Stankovic, T. Chau, C. Steele, E. Sejdic, Time-frequency analysis and Hermite projection method applied to swallowing accelerometry signals, EURASIP J. Adv. Signal Process. 2010 (2010), https://doi.org/10.1155/2010/323125.
[23] I. Orovic, S. Stankovic, T. Thayaparan, L. Stankovic, Multiwindow s-method for instantaneous frequency estimation and its application in radar signal analysis, IET Signal Process. (2010) 363–370, https://doi.org/10.1049/iet-spr.2009.0059.
[24] I. Orovic, N. Zaric, S. Stankovic, M. Amin, A multiwindow time-frequency approach based on the concepts of robust estimate theory, in: 2011 IEEE International Conference on Acoustics, Speech and Signal Processing (ICASSP), 2011, pp. 3584–3587.
[25] I. Orović, S. Stanković, M. Amin, A new approach for classification of human gait based on time-frequency feature representations, Signal Process. 91 (2011) 1448–1456, https://www.sciencedirect.com/science/article/pii/S0165168410003506, https://doi.org/10.1016/j.sigpro.2010.08.013, Fourier Related Transforms for Non-Stationary Signals.
[26] A. Sandryhaila, S. Saba, M. Püschel, J. Kovacevic, Efficient compression of QRS complexes using Hermite expansion, IEEE Trans. Signal Process. 60 (2012) 947–955, https://doi.org/10.1109/TSP.2011.2173336.
[27] M. Sandsten, J. Sandberg, Optimization of weighting factors for multiple window spectrogram of event-related potentials, EURASIP J. Adv. Signal Process. 2010 (2010), https://doi.org/10.1155/2010/391798.
[28] D. Selimović, J. Lerga, J. Prpić-Oršić, S. Kenji, Improving the performance of dynamic ship positioning systems: a review of filtering and estimation techniques, J. Marine Sci. Eng. 8 (2020), https://www.mdpi.com/2077-1312/8/4/234, https://doi.org/10.3390/jmse8040234.
[29] D. Slepian, H.O. Pollak, Prolate spheroidal wave functions, Fourier analysis and uncertainty – I, Bell Syst. Tech. J. 40 (1961) 43–63, https://doi.org/10.1002/j.1538-7305.1961.tb03976.x.
[30] L. Stankovic, A method for time-frequency analysis, IEEE Trans. Signal Process. 42 (1994) 225–229, https://doi.org/10.1109/78.258146.
[31] L. Stankovic, T. Thayaparan, V. Popović-Bugarin, I. Djurovic, M. Dakovic, Adaptive s-method for sar/isar imaging, EURASIP J. Adv. Signal Process. 2008 (2007), https://doi.org/10.1155/2008/593216.
[32] G. Szegő, Orthogonal Polynomials, 3rd ed., AMS Colloquium Publications, New York, USA, 1967.
[33] D.J. Thomson, Spectrum estimation and harmonic analysis, Proc. IEEE 70 (1982) 1055–1096, https://doi.org/10.1109/PROC.1982.12433.

Denis Selimović is currently pursuing a Ph.D. degree in Computer Science at the Faculty of Engineering, University of Rijeka, Croatia. He is also a member of the Center for Artificial Intelligence and Cybersecurity, University of Rijeka, Croatia. His main research interests include digital signal processing, machine learning, and artificial intelligence applications.

Jonatan Lerga received a Ph.D. degree from the Faculty of Electrical Engineering and Computing, University of Zagreb, Croatia, in 2011. He is currently an Associate Professor at the Faculty of Engineering, University of Rijeka, Croatia, where he is the Head of the Department of Computer Engineering and the Information Processing Laboratory. He is also the Head of the Center for Artificial Intelligence and Cybersecurity, University of Rijeka, Croatia. He published more than 70 scientific papers with 35 papers in WoS journals. His main research interests include digital signal and image processing, artificial intelligence applications, information theory, and coding. Prof. Lerga received numerous awards for his work: the Annual Award of the Croatian Academy of Engineering for his scientific achievements in 2012, the Annual Award of the City of Rijeka in 2015, and the Annual Award of the Primorje-Gorski Kotar County in 2018. Also, he received several recognitions from the Foundation of the University of Rijeka, in 2008, 2010, and 2018.

Péter Kovács received his Ph.D. in computer science from the Eötvös Loránd University (ELTE), Budapest, Hungary, in 2016. His research interests include signal processing, numerical analysis, and optimization. Since 2016 he has been an assistant professor at the Department of Numerical Analysis of ELTE. He spent five months as visiting researcher at the Department of Signal Processing, the Tampere University of Technology in Finland, and 30 months as a postdoc at the Institute of Signal Processing, Johannes Kepler University Linz in Austria. In 2016 he received the Farkas Gyula Prize in applied mathematics from the János Bolyai Mathematical Society. In 2022 he was habilitated at the Faculty of Informatics of ELTE.

Jasna Prpić-Oršić was born in 1965 in Rijeka, Croatia. She is a professor at the Department of Naval Architecture and Ocean Engineering, Faculty of Engineering, University of Rijeka, and the Head of the Ship Dynamics Chair. She has served as Dean of the Faculty of Engineering (2016-2019) and Vice Dean for Research Affairs (2010-2016). She has been a visiting researcher on NTNU since 2008, at the Center of Ships and Ocean Structures (CESOS) and the Centre for Autonomous Marine Operations and Systems (AMOS), Norwegian Centers of Excellence, Trondheim, Norway. She is also an associate researcher at the Centre for Marine Technology and Ocean Engineering, Group of Marine Dynamics and Hydrodynamics, Instituto Superior Tecnico, Lisbon, Portugal. She has been a member of IMAM (International Maritime Association of the Mediterranean) since 2011 and was President of IMAM (2015-2017). She has been a member of the ISSC Loads Committee since 2015. She has been a lead researcher on eight scientific projects. Currently, she is the lead researcher of the project Decision Support System for Green and Safe Ship Routing, funded by the Croatian Foundation for Research. She received the Republic of Croatia Annual Scientific Award in 2020 and the Croatian Academy of Sciences and Arts Award in 2007. She has published some 150 scientific papers and two books. Her main interests include seakeeping, numerical simulations in marine dynamics, wave loads, and the response of marine objects.